

**Electronic Supplementary Information (ESI) for**

**High energy density hybrid Mg<sup>2+</sup>/Li<sup>+</sup> battery with superior ultra-low temperature performance**

Zhonghua Zhang,<sup>1,2</sup> Huimin Xu<sup>3</sup> Zili Cui,<sup>1</sup> Pu Hu,<sup>1</sup> Jingchao Chai,<sup>1</sup> Huiping Du,<sup>1</sup> Jianjiang He,<sup>1</sup>

Jianjun Zhang,<sup>1</sup> Xinhong Zhou,<sup>3</sup> Pengxian Han,<sup>1</sup> Guanglei Cui\*,<sup>1</sup> & Liquan Chen<sup>4</sup>

<sup>1</sup>*Qingdao Industrial Energy Storage Research Institute, Qingdao Institute of Bioenergy and Bioprocess Technology, Chinese Academy of Sciences, Qingdao, 266101, P. R. China.*

<sup>2</sup>*University of Chinese Academy of Sciences, Beijing 100190, P.R. China.*

<sup>3</sup>*College of Chemistry and Molecular Engineering, Qingdao University of Science and Technology, Qingdao, 266042, P. R. China.*

<sup>4</sup>*Beijing National Laboratory for Condensed Matter Physics, Institute of Physics, Chinese Academy of Sciences, Beijing 102488, P.R. China.*

*\*Corresponding authors. Tel.: 86-532-80662746; fax: 86-532-80662746. E-mail: cuigl@qibebt.ac.cn*

**This PDF file includes:**

- 1. Fig. S1 to Fig. S9**
- 2. Tab. S1 and Tab. S2**
- 3. Supplementary References**

## 1. Supplementary Figures

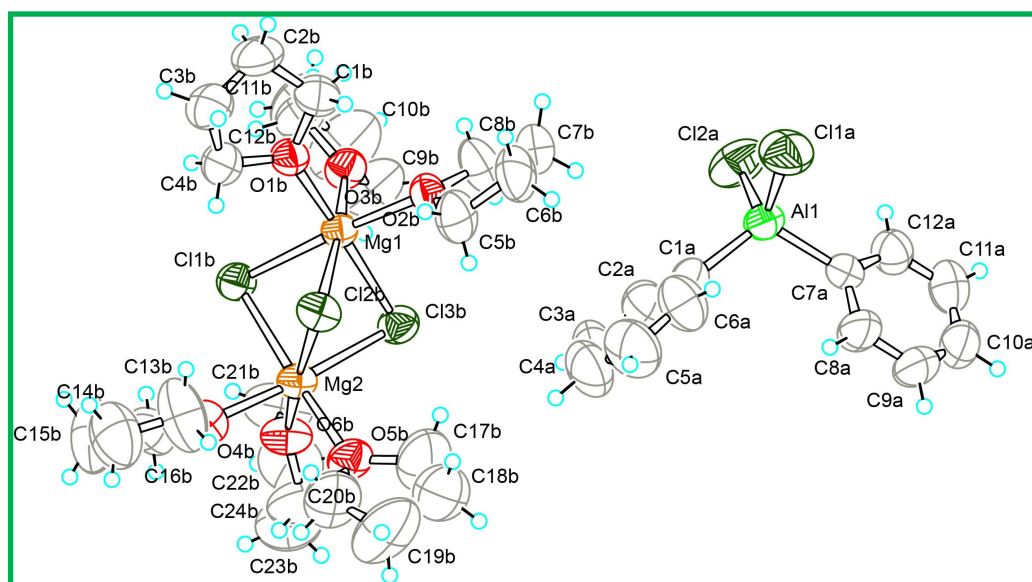


**Fig. S1** Structure of the crystallized product from the THF solution of PhMgCl-MgCl<sub>2</sub>.

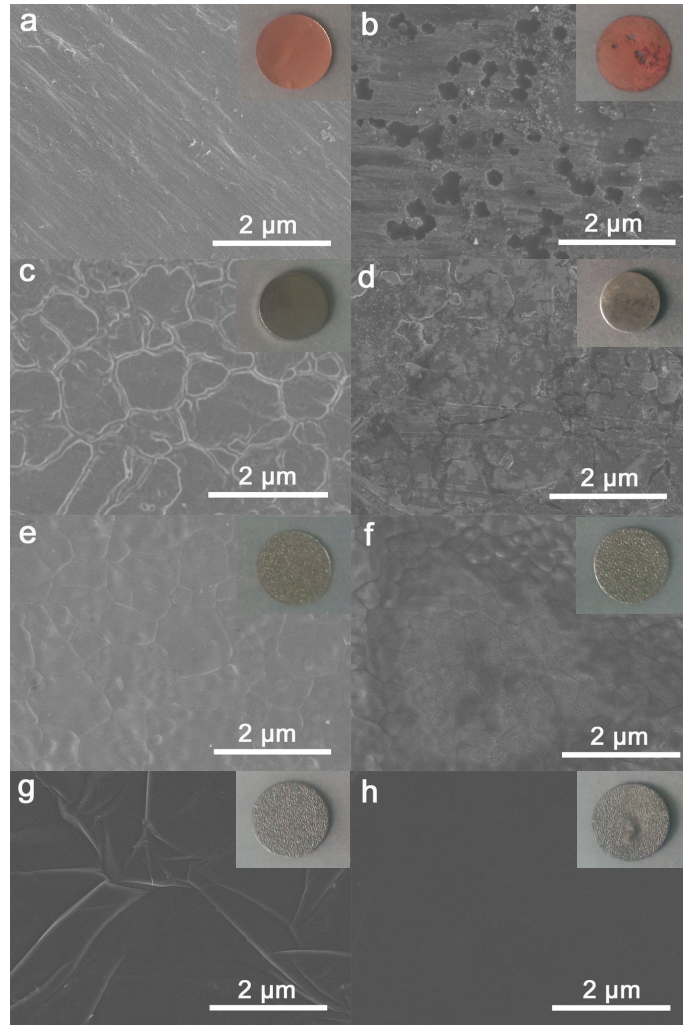


**Fig. S2** Typical SEM images and digital photos (insets) of various current collectors before (a, c, e, and g) and after (b, d, f, and h) galvanostatic discharge-charge experiments (Cu: a and b; SS: c and d; Ni: e and f; GF: g and h).

In order to authenticate the corrosion of various non-metal current collectors, there is a direct comparison of their SEM images and digital photos (Fig. S2) before and after galvanostatic discharge-charge experiments. The relative smooth surfaces of Cu and stainless steel electrodes suffer from severe corrosion and electrode deteriorations during the galvanostatic discharge-charge experiments, as depicted in Fig. S2b and S2d. The intact circular Cu electrode becomes decayed with visible apertures, while black spots can be clearly observed on the surfaces

of stainless steel electrode. Ni electrode undergoes mild pitting corrosion tendency, whose surface exhibits less notable change compared to that of Cu and stainless steel electrodes after galvanostatic discharge-charge experiments. However, no surface morphology changes are observed (Fig. S2g and S2h) for the graphite film from both microcosmic and macroscopical view, indicating that graphite film is electrochemically stable over the tested potential range due to the nonoccurrence of undesirable side-reactions.

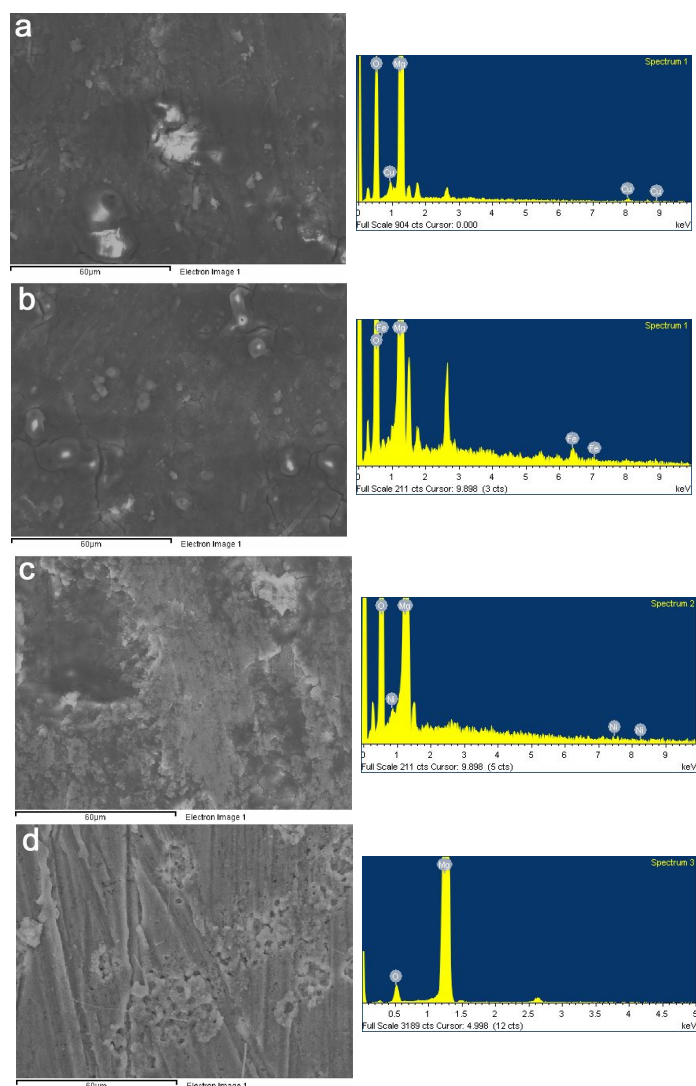


**Fig. S3** SEM images and corresponding EDS results of Mg metal anodes coupled with Cu (a), SS (b), Ni (c), and GF (d) working electrode after the galvanostatic discharge-charge experiments.

The shuttle effects of various non-noble metal ions are examined by EDS analysis. Fig. S3 depicts the morphologies and elements compositions of Mg anode after CV tests. Obviously, after the galvanostatic discharge-charge tests the surface of Mg electrode becomes rough and is covered by solid layers. When coupled with the non-noble metal working electrode, their EDX analysis reveals that these solid layers are comprised of a large fraction of non-noble metal ions. As for the GF working electrode, their counter Mg electrode contains two elements (i.e. Mg and O), suggesting that GF are much more stable in the APC electrolyte than non-noble metals. Here the

trace amount of oxygen may be derived from the oxidation of Mg anode when the electrode is transferred into chamber of the microscope. It is concluded that the non-noble metals are oxidated into metal ions during charging and then diffuse to anode, followed by depositing on the Mg surface via direct replacement reactions. These results are in accordance with previous reports.<sup>1-3</sup>

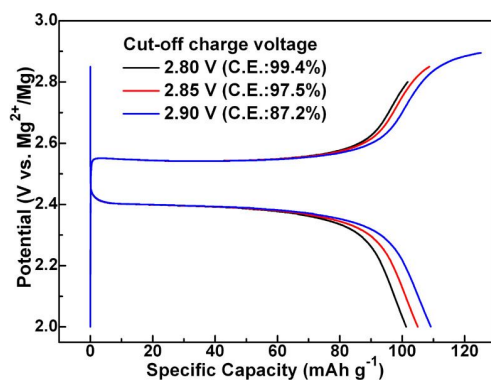


**Fig. S4** Galvanostatic discharge-charge curves of the hybrid Mg<sup>2+</sup>/Li<sup>+</sup> batteries with different cut-off charge voltages obtained at 170 mA g<sup>-1</sup> in a pouch cell confirmation.

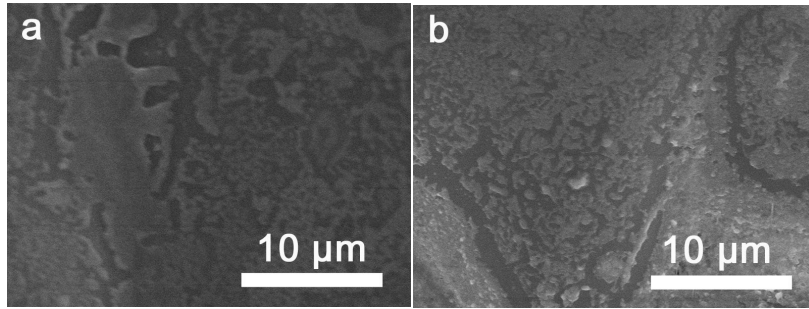


**Fig. S5** Typical SEM images of the Mg anode obtained from the hybrid  $\text{Mg}^{2+}/\text{Li}^+$  batteries charged at 0.15 C (a) and 3.0 C after 10 cycles (b).

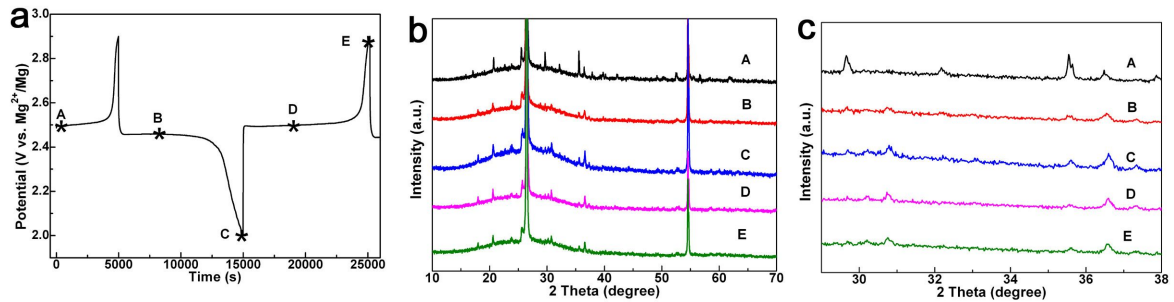


**Fig. S6** Galvanostatic discharge-charge curves (a) of the LFP@GF electrode during the first discharge and charge process; Ex situ XRD patterns (b and c) from points A to E. The sharp and intense peaks at  $26.6^\circ$  and  $54.7^\circ$  are indexed to be the (002) and (004) peak of typical graphite.

In an effort to uncover the working mechanism of the hybrid  $\text{Mg}^{2+}/\text{Li}^+$  battery, further studies on the phase transitions during discharge and charge are carried out via ex situ XRD experiments (Fig. S6). The two-phase  $\text{Li}^+$  ions intercalation/deintercalation process is obviously characterized by a flat charge and discharge profile and a phase evolution from XRD patterns, which is in accordance with previous reports.<sup>5</sup>

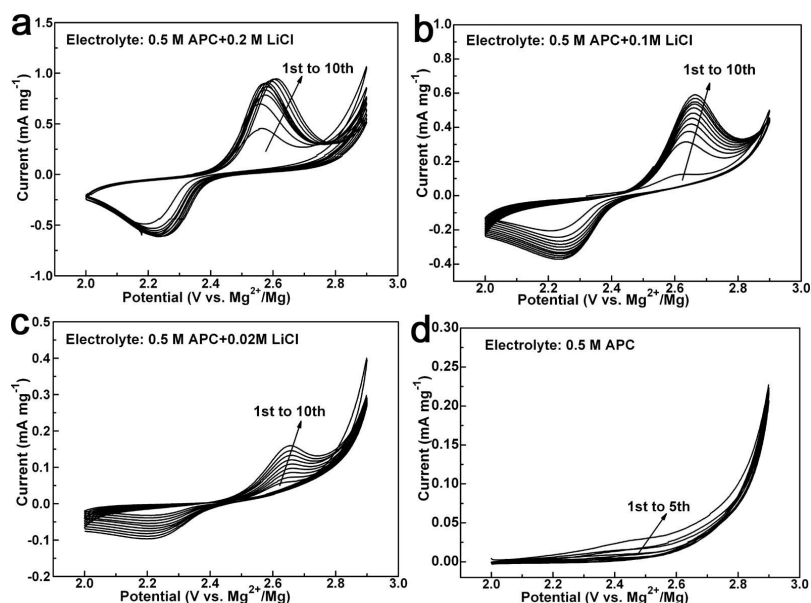


**Fig. S7** CV curves of the hybrid  $\text{Mg}^{2+}/\text{Li}^{+}$  battery in the APC electrolytes with different amounts of LiCl at a scan rate of  $1 \text{ mV s}^{-1}$  (a: 0.2 M, b: 0.1 M, c: 0.01 M, and d: 0 M).

Further decreasing  $\text{Li}^{+}$  ions' concentration in hybrid electrolytes engenders worse reproducibility of the sequent CV curves (Fig. S7a to S7d). As for the pristine APC electrolytes (Fig. S7d), there is no obvious anodic and cathodic peaks, indicating an irreversible electrochemical reaction. It is noteworthy that the LFP@GF electrodes present different electrochemical behavior from the traditional  $\text{Mo}_6\text{S}_8$  electrode when they are evaluated at a relatively low LiCl concentration of 0.02 M, which may be caused by the  $\text{Li}^{+}$  and  $\text{Mg}^{2+}$  co-intercalation reaction occurred at the  $\text{Mo}_6\text{S}_8$  cathode, while only the  $\text{Li}^{+}$  intercalation can take place at the LFP@GF cathode due to the strong electrostatic interactions between  $\text{PO}_4^{3-}$  anions and  $\text{Mg}^{2+}$  ions.



**Fig. S8** A line linkage image between hybrid batteries and electric fan (left); An electric fan is powered by two hybrid  $\text{Mg}^{2+}/\text{Li}^{+}$  pouch devices at varied low temperature of 0 (middle up), -10 (right up), -20 (middle down), and -40 °C (right down).

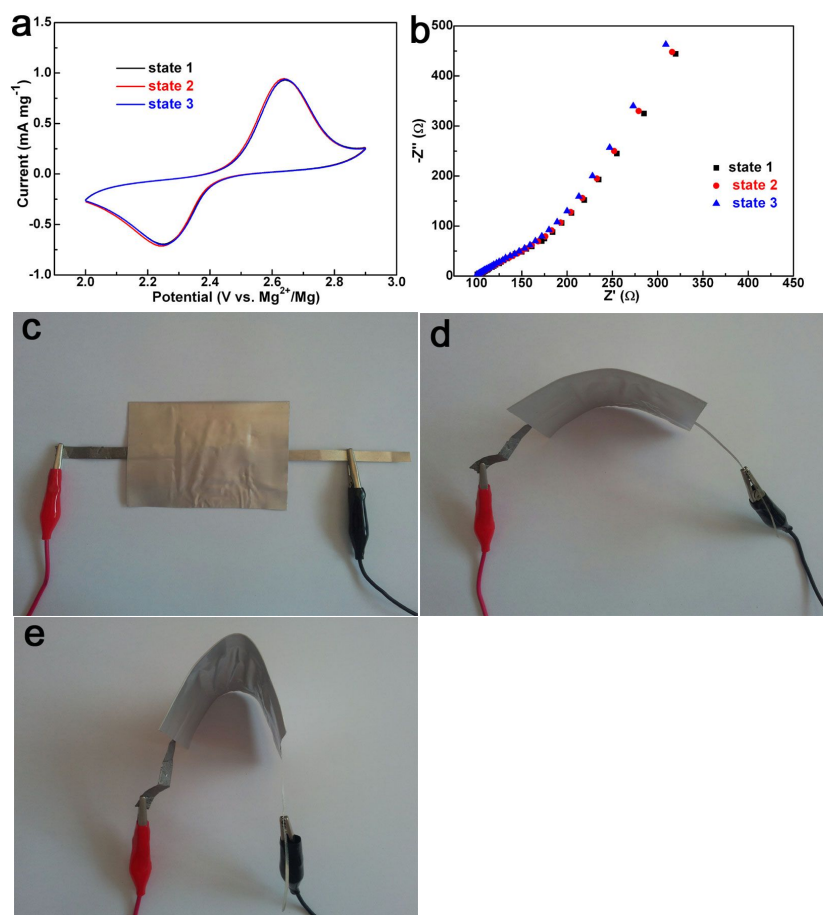


**Fig. S9** CV (a) and EIS (b) results of the hybrid  $\text{Mg}^{2+}/\text{Li}^{+}$  battery at flat (c), and modest (d) and largest (e) bending states.

To illustrate the flexibility of the LFP@GF electrode, the hybrid  $\text{Mg}^{2+}/\text{Li}^{+}$  device is placed in flat and two bending states to evaluate its electrochemical performance by CV and EIS measurements. It shows perfectly overlapped CV curves (Fig. S9a) and negligible impedance increase (Fig. S9b) at different bending states (Fig. S9c to S9e), indicating the excellent mechanical stability and flexibility of the hybrid  $\text{Mg}^{2+}/\text{Li}^{+}$  devices.

## 2. Supplementary Tables

**Tab. S1** The over-potential, peak area and efficiency data of the graphite film electrode during Mg deposition/dissolution processes obtained from CV curves.

Cycle	Over-potential (V)		Peak area		Efficiency
	Deposition	Dissolution	Deposition	Dissolution	
1	-0.48	0.13	0.00254	0.00237	93.3%
2	-0.47	0.12	0.00352	0.00335	95.2%
3	-0.39	0.08	0.00487	0.00471	96.8%

**Tab. S2** Electrochemical performance comparison of the hybrid Mg<sup>2+</sup>/Li<sup>+</sup> batteries of previously reported cathodes and electrolytes.

Cathodes	Electrolytes	Average potential (V vs. Mg <sup>2+</sup> /Mg)	Current density (mA g <sup>-1</sup> )	Cycling performance		Rate capability, mAh g <sup>-1</sup> (current density, mA g <sup>-1</sup> )		Reference
				Initial Capacitance (mAh g <sup>-1</sup> )	Capacity retention (cycle number)			
Mo <sub>6</sub> S <sub>8</sub>	DCC/LiCl	1.3	12.8	113	-	-	-	7
Mo <sub>6</sub> S <sub>8</sub>	Mg(BH <sub>4</sub> ) <sub>2</sub> /LiBH <sub>4</sub>	1.3	12.8	99.5	89.7% (300)	-	-	8
Mo <sub>6</sub> S <sub>8</sub>	APC/LiCl	1.3	30.5	120	96.4% (100)	114 (2440)	106 (3660)	4
Mo <sub>6</sub> S <sub>8</sub>	APC/LiCl	1.3	12.8	126	95% (3000)	110 (640)	105 (1920)	9
TiS <sub>2</sub>	APC/LiCl	1.4	80	160	99.5% (400)	100 (240)	65 (480)	10
TiS <sub>2</sub>	APC/LiCl	1.4	24.0	220	95% (2000)	125 (2400)	50 (4800)	11
TiO <sub>2</sub>	Mg(BH <sub>4</sub> ) <sub>2</sub> /LiBH <sub>4</sub>	0.9	33.6	155.8	89.8% (90)	123 (168)	85 (336)	12
Li <sub>4</sub> Ti <sub>5</sub> O <sub>12</sub>	APC/LiCl	0.7	15	190	100% (100)	130 (150)	110 (300)	13
*V <sub>2</sub> O <sub>5</sub>	APC/LiCl	2.3	-	130	-	-	-	17
S	Mg-HMDS / LiTFSI	1.5	71	1000	-	-	-	14
*LiFePO <sub>4</sub>	APC/LiBF <sub>4</sub>	2.4	17	124	-	-	-	5
*LiFePO <sub>4</sub>	APC/aqueous Li <sub>2</sub> SO <sub>4</sub>	2.1	50	121.7	90%(20)	-	-	15
*LiMn <sub>2</sub> O <sub>4</sub>	Al(OPh) <sub>3</sub> / PhMgCl / LiPF <sub>6</sub>	-	74	100	80% (20)	-	-	16
Our work LiFePO <sub>4</sub>	APC/LiCl	2.45	25.5	156	98.5% (200)	96.6 (204)	68.8 (510)	

\* represent unsuccessful cell assembly in two electrode system; DCC means dichloro-complex.

### 3. Supplementary References

1. S. Partha, K. D. Moni, I. V. Oleg, M. Ayyakkannu, A. David, N. K. Prashant, *Prog. Mater. Sci.* **2014**, *66*, 1–86.
2. D. Lv, T. Xu, P. Saha, M. K. Datta, M. L. Gordin, A. Manivannan, P. N. Kumta, D. Wang, *J. Electrochem. Soc.* **2013**, *160*, A351–A355.
3. S. Yagi, A. Tanaka, Y. Ichikawa, T. Ichitsubo, E. Matsubarab, *J. Electrochem. Soc.* **2013**, *160*, C83–C88.
4. J. Cho, M. Aykol, S. Kim, J. Ha, C.. Wolverton, K. Y. Chung, K. Kim, B. Cho, *J. Am. Chem. Soc.* **2014**, *136*, 16116–16119.
5. S. Yagi, T. Ichitsubo, Y. Shirai, S. Yanai, T. Doi, K. Muraseb, E. Matsubar, *J. Mater. Chem. A* **2014**, *2*, 1144–1149.
6. P. Gibot, M.Casas-Cabanas, L. Laffont, S. Levasseur, P. Carlach, S. Hamelet, J. M. Tarascon, C. Masquelier, *Nat. Mater.* **2008**, *7*, 741–747.
7. Y. Gofer, O. Chusid, H. Gizbar, Y. Viestfrid, H. E. Gottlieb, V. Marks, D. Aurbach, *Electrochem. Solid-State Lett.* **2006**, *9*, A257–A260.
8. Y. Shao, T. Liu, G. Li, M. Gu, Z. Nie, M. Engelhard, J. Xiao , D. Lv, C. Wang, J. G. Zhang, J. Liu, *Sci. Rep.* **2013**, *3*, 3130.
9. Y. Cheng, Y. Shao, J. Zhang, V. L. Sprenkle, J. Liu, G. Li, *Chem. Commun.* **2014**, *50*, 9644–9646.
10. T. Gao, F. Han, Y. Zhu, L. Suo, C. Luo, K. Xu, C. Wang, *Adv. Energy Mater.* **2014**, 1401507.
11. H. D. Yoo, Y. Liang, Y. Li, Y. Yao, *ACS Appl. Mater. Interfaces* **2015**, *7*, 7001–7007.
12. S. Su, Z. Huang, Y. NuLi, F. Tuerxun, J. Yang, J. Wang, *Chem. Commun.* **2015**, *51*, 2641–2644.

13. N. Wu, Z. Yang, H. Yao, Y. Yin, L. Gu, Y. Guo, *Angew. Chem. Int. Ed.* **2015**, *54*, 1–6.
14. T. Gao, M. Noked, A. J. Pearse, E. Gillette, X. Fan, Y. Zhu, C. Luo, L. Suo, M. A. Schroeder, K. Xu, S. B. Lee, G. W. Rubloff, C. Wang, *J. Am. Chem. Soc.* DOI: 10.1021/jacs.5b07820.
15. Z. Chang, Y. Yang, X. Wang, M. Li, Z. Fu, Y. Wu, R. Holze, *Sci. Rep.* **2015**, *5*, 11931.
16. E. G. Nelson, S. I. Brody, J. W. Kampf, B. M. Bartlett, *J. Mater. Chem. A* **2014**, *2*, 18194–18198.
17. H. D. Yoo, I. Shterenberg, Y. Gofer, G. Gershinsky, N. Pour, D. Aurbach, *Energy Environ. Sci.* **2013**, *6*, 2265–2279.